



A study of climate model responses of the western Pacific subtropical high to El Niño diversity

Mengyan Chen^{1,2} · Ting-Huai Chang³ · Ching-Teng Lee³ · Shih-Wei Fang² · Jin-Yi Yu²

Received: 29 March 2020 / Accepted: 9 October 2020 / Published online: 19 October 2020
© Springer-Verlag GmbH Germany, part of Springer Nature 2020

Abstract

This study examines a climate model hindcast of the responses of the western Pacific subtropical high (WPSH) to three types of El Niño events: the Eastern Pacific (EP) El Niño and the types I and II of Central Pacific (CP-I and CP-II) El Niño. These El Niño types differ from each other in the central locations and patterns of their sea surface temperature (SST) anomalies. They invoke four different mechanisms to impact the WPSH. Hindcasts produced by the Taiwan Central Weather Bureau (CWB) Climate Forecast System 1-tiered model (TCWB1T1) are analyzed. These hindcasts realistically simulate the impacts on the WPSH during the CP-I El Niño, but overestimate the impacts during the decaying summer of the EP El Niño and during the developing autumn and early winter of the CP-II El Niño. The overestimates are mainly the result of an overly strong Maritime Continent regional circulation mechanism during EP El Niños and an overly strong Indian Ocean capacitor mechanism during CP-II El Niños. Further analyses show that these model biases are related to biases in the simulations of El Niño SST anomalies and the Walker circulation. Both model deficiencies are common to contemporary coupled climate models.

Keywords Western Pacific subtropical high · EP El Niño · CP-I El Niño · CP-II El Niño · Forecast

1 Introduction

The western Pacific subtropical high (WPSH) is one of the most influential atmospheric circulation systems impacting East Asian and western Pacific weather and climate. The location and intensity of the WPSH have an impact on, for example, typhoon tracks and landfall locations (e.g., Du et al. 2011; Ho et al. 2004; Wu et al. 2005; Stowasser et al. 2007) and the intensity of the Indian and Asian monsoons (e.g., Lau et al. 2000; Chang et al. 2000; Wang et al. 2000; Lee et al. 2005; Park et al. 2010; Matsumura et al. 2015). Inter-annual variations in the WPSH are closely linked to El Niño-Southern Oscillation (ENSO) events (e.g., Jiang et al. 2017, 2018; Kumar and Hoerling 2003; Paek et al. 2015,

2019; Park et al. 2010; Sui et al. 2007; Wang et al. 2000; Wang and Zhang 2002; Xie et al. 2009, 2016). The WPSH tends to intensify during the mature and decaying phases of El Niño events (Wang et al. 2000; Wang and Zhang 2002; Xiang et al. 2013; Xie et al. 2009, 2016). Various mechanisms have been proposed to explain these El Niño impacts on the WPSH. Wang et al. (2000) linked these impacts to local atmosphere–ocean coupling in the Northwestern Pacific (NWP) triggered by a Rossby wave response to the El Niño sea surface temperature (SST) anomalies. Xie et al. (2009) linked the El Niño impacts to an Indian Ocean capacitor mechanism, in which the El Niño-induced Indian Ocean warming excites Kelvin wave propagation to strengthen the WPSH during the decaying summer of El Niño. Sui et al. (2007) suggested that El Niño-related convection and SST anomalies around the Maritime continent (MC) can affect the WPSH via a local meridional circulation connecting the MC and the WPSH.

Based on the locations of the maximum SST anomalies, researchers have separated El Niño events into Eastern Pacific (EP) and Central Pacific (CP) types (Kao and Yu 2009; Yu and Kao 2007). Chen et al. (2019) finds that the NWP local coupling mechanism of Wang et al. (2000)

✉ Jin-Yi Yu
jyyu@uci.edu

¹ State Key Laboratory of Tropical Oceanography, South China Sea Institute of Oceanology, Chinese Academy of Sciences, Guangzhou, China

² Department of Earth System Science, University of California, Irvine, CA, USA

³ Central Weather Bureau, Taipei, Taiwan

can be activated either by two consecutive Gill responses to SST anomalies in the tropical eastern Pacific (e.g., the EP El Niño) or a single Gill response to SST anomalies in the tropical central Pacific (e.g., the CP El Niño). They referred to these two mechanisms, respectively, as the NWP-II and NWP-I local coupling mechanisms and used them to understand the WPSH responses to El Niño diversity. With the NWP-II (two-step Gill response) mechanism, warm SST anomalies in the tropical eastern Pacific can excite a Gill response to produce an anomalous cyclone to the west of the SST anomalies. The anomalous cyclone then enhances the northeast trade winds to subsequently induce cold SST anomalies in the subtropical central Pacific. The cold anomalies can then excite a second Gill type response to establish an anomalous anticyclone in the NWP region. With the NWP-I (one-step Gill response) mechanism, positive SST anomalies in the tropical central Pacific excite a Gill response to directly establish an anomalous cyclone over the NWP region.

Recent studies suggested that the CP El Niño needs to be further divided into CP-I and CP-II types due to differences in their SST evolution patterns (Wang and Wang 2013) and climate impacts (Wang and Wang 2013; Tan et al. 2016; Chen et al. 2019). While the CP-I and CP-II El Niños are both characterized by having their largest positive SST anomalies in the equatorial central Pacific, the origins and spatial patterns of their SST anomalies are noticeably different. The SST anomalies of the CP-I El Niño originate and develop locally in the equatorial central Pacific, while the SST anomalies of the CP-II El Niño originate from the northeastern subtropical Pacific. The SST anomalies exhibit a symmetric distribution pattern about the equator for the CP-I El Niño but an asymmetric distribution pattern for the CP-II El Niño during their peak phases.

Chen et al. (2019) analyzed reanalysis data to find that the El Niño impacts on the WPSH are distinctly different among the EP, CP-I, and CP-II types. They find that the EP El Niño impacts the WPSH most strongly from the developing autumn to decaying summer via the NWP mechanism of Wang et al. (2000) and the Indian Ocean capacitor mechanism of Xie et al. (2009). The CP-II El Niño exerts a stronger impact on the WPSH than the EP El Niño while CP-I El Niño exerts a weaker impact. The CP-II El Niño's impact persists from its developing summer into decaying summer through the MC circulation mechanism of Sui et al. (2007), while the CP-I El Niño's impact is only significant during its peak winter through the NWP mechanism. The results from Chen et al. (2019) indicate that the conventional view on how El Niño impacts the WPSH needs to be revised to take into account El Niño diversity.

It is important for climate models to simulate the different impacts and impact mechanisms in order to produce skillful predictions of WPSH variations during El Niño events. It is

also important to know what the causes are for the model deficiencies in the simulations. In this study, we examine retrospective hindcasts produced by a weather forecast agency for the aforementioned purposes. We choose to use the hindcasts produced by the Taiwan Central Weather Bureau Climate Forecast System 1-tiered model (TCWB1T1) due to its availability to us. Also, as we elaborate on later, many of the model deficiencies we identify from this model are common to other climate models. Results obtained using the CWB model can be useful to other modelling groups as well. The rest of this study is organized as follows. Section 2 describes the observational datasets, the retrospective hindcasts, and the TCWB1T1 model used in this study. Section 3 describes the performance of the CWB model in simulating the WPSH and the impact mechanisms characteristic of the three types of El Niño. Section 4 examines the sources of model deficiencies. A set of conclusions and a discussion are presented in Sect. 5.

2 Data and methods

Nine-month hindcasts produced by the TCWB1T1 model (Wu et al. 2019) are used. The TCWB1T1 is a coupled atmosphere–ocean model that consists of the CWB Global Forecast System as the atmospheric model component and the Modular Ocean Model version 3 (MOM3) as the oceanic model component. The hindcast period is from January 1982 to December 2011. For each month, hindcasts were launched at days 1, 3, 6, 8, 11, 13, 16, 18, 21, and 23, resulting in 10-member ensembles. The lead-0 to lead-9 month hindcasts are the monthly averages of these daily predictions (i.e., the 10-member ensembles). The monthly anomalies are defined as the deviations from the hindcasts monthly climatology after removing linear trends. The model was shown to have reasonable skills in sub-seasonal to seasonal forecasts (Wu et al. 2019). The pattern correlation coefficient between the 1-month hindcasted and observed SST anomalies in the global oceans is significant at 95% confidence level. While the correlation decreases as the increase of the lead time, the correlation coefficient at the 2-month lead remain significant in most of the tropical oceans.

Observational datasets used in this study include monthly SSTs from the Hadley Centre Sea Ice and SST dataset (HadISST) (Rayner et al. 2003) at a horizontal resolution of $1.0^\circ \times 1.0^\circ$, and monthly mean sea level pressure (SLP), winds and vertical velocities from the National Centers for Environmental Prediction/National Center for Atmospheric Research Reanalysis 1 with a horizontal resolution of $2.5^\circ \times 2.5^\circ$ (Kalnay et al. 1996). For the purposes of model verification, the analysis period of all observational datasets is the same as that of the TCWB1T1 hindcasts, January 1982 to December 2011. Anomalies in the observations are

defined as the deviations from the observed monthly climatology after removing linear trends.

The categorization of El Niño events is based on Chen et al. (2019). During the analysis period, there are two EP El Niño events (1982/1983, 1997/1998), three CP-I El Niño events (1987/88, 1990/1991, 2002/2003), and four CP-II El Niño events (1991/1992, 1992/1993, 2004/2005, 2009/2010).

Several indices are used in this study. The WPSH index from Paek et al. (2015) is used to quantify variations in the strength of the WPSH. This index is defined as the SLP anomalies area-averaged over northwestern Pacific (10° – 30° N, 120° – 160° E). The Cold Tongue Index (CTI) is used to represent El Niño intensity and is defined as the area averaged SST anomalies over the equatorial Pacific (5° S– 5° N, 180° – 90° W). Four mechanism indices defined in Chen et al. (2019) are used to quantify the mechanisms that enable El Niño to impact WPSH. These indices are the Indian Ocean capacitor (IOC) index, the MC index, the NWP-I index, and the NWP-II index. The IOC index is defined as the SST anomalies averaged over the tropical north Indian Ocean (5 – 25° N, 40 – 100° E) following Xie et al. (2009). The MC index is defined as the difference in 850-hPa vertical velocity between the WPSH index region and the maritime continent

region (20° S– 10° N, 110° – 150° E). The NWP-I index is defined as the SST anomalies averaged over the tropical central Pacific Ocean (10° S– 10° N, 160° – 180° E) multiplied by -1 . The NWP-II index is defined as the SST anomalies over the subtropical central Pacific (10 – 20° N, 150° – 170° E) multiplied by -1 . As explained in Chen et al. (2019), the NWP-I and NWP-II indices are used respectively to quantify the local NWP coupling associated with the one-step and two-step Gill responses to El Niños.

3 Simulations of the El Niño impacts on the WPSH and the impact mechanisms

Figure 1 shows the differences between the hindcasted seasonal-mean SLPs and the observations at 0-, 3-, 6-, 9-month leads for target seasons of March–April–May (MAM), June–July–August (JJA), September–October–November (SON) and December–January–February (DJF). At a lead time of 0-month, where the model SSTs are still close to the observations, the SLP biases for the four seasons are less than -1 hPa in the northwestern Pacific (NWP). The SLP bias in that region increases with lead time and reaches about $+3$ hPa at 9-month leads for the four target seasons.

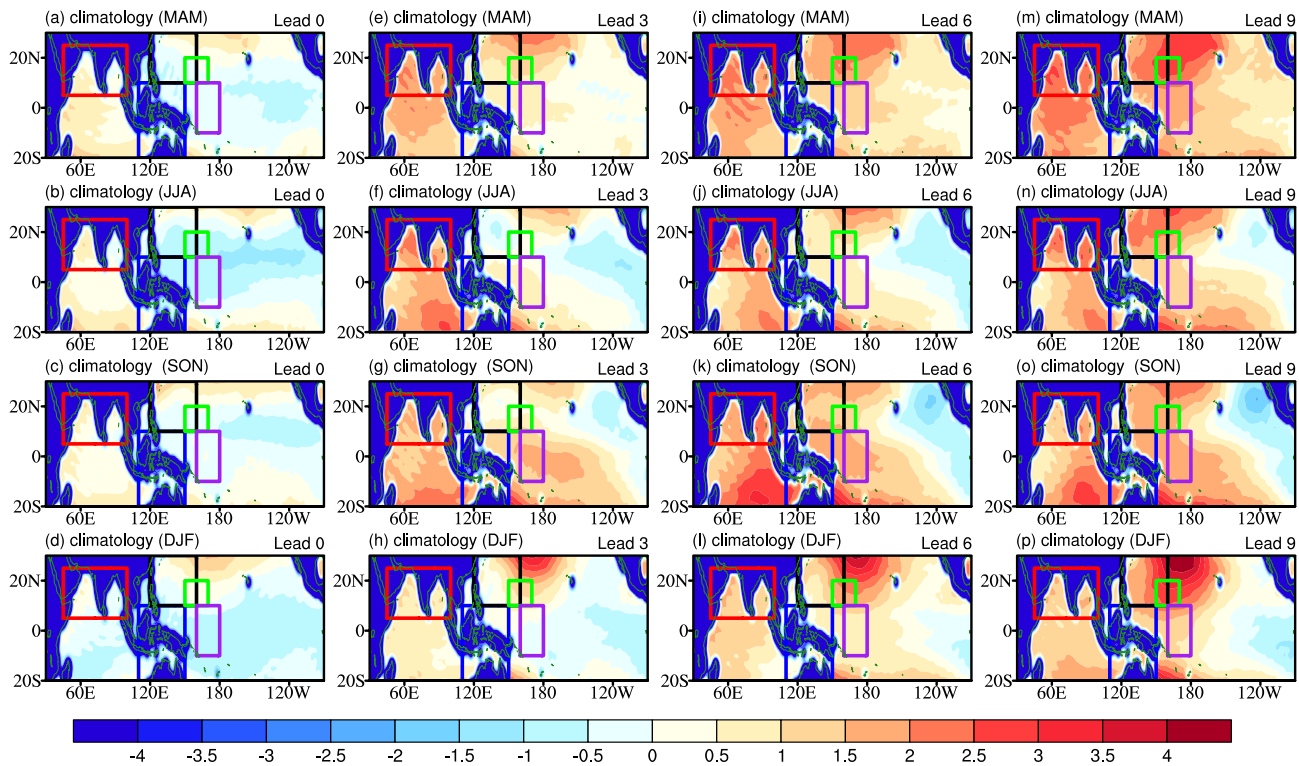


Fig. 1 Differences between hindcasted seasonal-mean SLPs and the observations calculated from the 0-month lead (1st column), 3-month lead (2nd column), 6-month lead (3rd column), and 9-month lead (4th column) hindcasts for target seasons of March–April–May (MAM; 1st row), June–July–August (JJA; 2nd row), September–October–November (SON; 3rd), and December–January–February (DJF; 4th row). The black boxes mark the region where the WPSH index is defined

(MAM; 1st row), June–July–August (JJA; 2nd row), September–October–November (SON; 3rd), and December–January–February (DJF; 4th row). The black boxes mark the region where the WPSH index is defined

The observed standard deviation of the WPSH index is about 0.76 hPa.

To evaluate the skill of the CWB hindcasts in predicting the WPSH variations associated with the El Niño, we compare in Fig. 2 the hindcasted and observed WPSH indexes composites for the three types of El Niño events. Values shown are the 3-month running means and have been standardized for the sake of comparison. To assess the overall performance of the hindcasts, we also show in

Fig. 2d–f the mean and spread (i.e., one standard deviation) of the WPSH index calculated from all 10 lead hindcasts. Figure 2a–c show that the WPSH indexes produced by the lead-0 hindcasts in general follow the observations for all types of El Niño. The results indicate that the atmospheric model component of the CWB model can realistically simulate the WPSH variations when forced with close-to-realistic SSTs. The biases in the hindcasted WPSH indices increase with the increasing lead time. Specifically, for the EP El

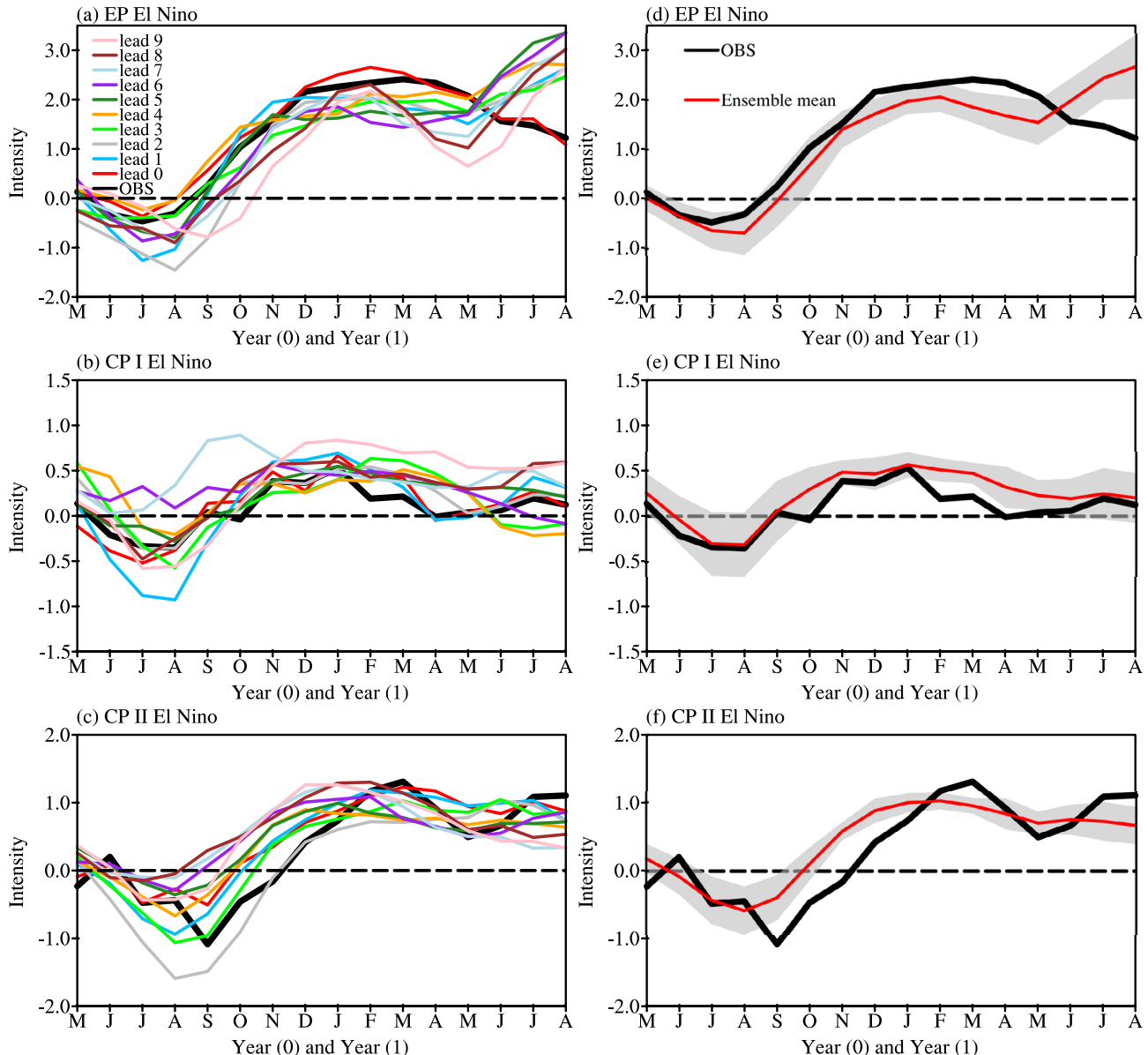


Fig. 2 Variations of composite western Pacific subtropical high (WPSH) index from the developing year (Year (0)) to decaying year (Year (1)) of the EP El Niño (top row), the CP-I El Niño (middle row), and the CP-II El Niño (bottom row). Composites calculated from the observations are represented in bold-black lines in all panels and from 0- month to 9-month lead are represented in thin-color lines

in left panels (a–c). The left panels represent the observations and outputs of CWB models at different lead time. In the right panels, the red lines and gray shading represent the means and standard deviation of the hindcast shown in the left panels. Values shown in all panels are the 3-month running means that have been standardized

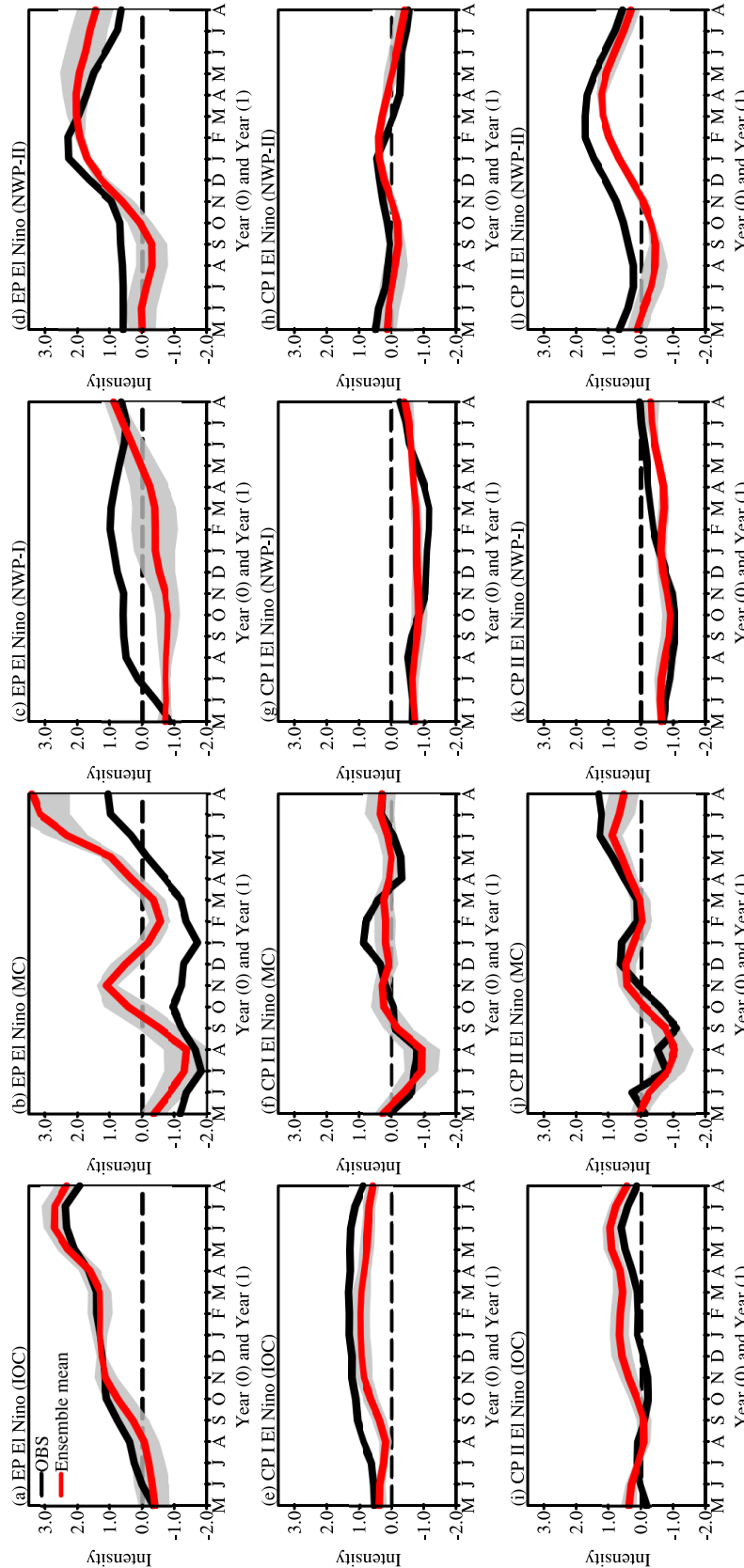


Fig. 3 Composite indices for the Indian Ocean capacitor (IOC) mechanism (the 1st column), Maritime continent (MC) circulation mechanism (the 2nd column), one-step Northwestern Pacific (NWP) coupling mechanism (NWP-I; the 3rd column), and the two-step NWP coupling mechanism (NWP-II; the 4th column) from the developing year (Year(0)) to the decaying year (Year(1)) of the EP El Niño (the first row), CP-I El Niño (the second row), and CP-II El Niño (the third row). Composites are colored black for observations and red for the means of the hindcasts from lead-0 to lead-9 months. Gray shadings indicate the range of one standard deviation calculated from the lead-0 to lead-9-month hindcasts. Values shown in all panels are the 3-month running means that have been standardized

Niño, the hindcasted WPSH index follows the observed one during the developing and peak phases (i.e., May through next February) and decaying spring but is overestimated during the decaying summer at all lead times except lead-0. This general characteristic is clearly reflected in Fig. 2d, which shows that the mean forecasted WPSH aligns with the observations throughout the lifecycle of EP El Niño except during the decaying summer. For the CP-I El Niño, except at the 6 and 7-month leads, the hindcasted WPSH index follows the variation pattern of the observed WPSH index throughout the lifecycle (Fig. 2b, e). For the CP-II El Niño, the hindcasted WPSH index is close to the observed one except during the developing autumn-to-early winter and at

the 2-month lead (Fig. 2c, f). The ensemble means of different lead times (Fig. 2f) clearly exhibits this feature. The hindcasts produce overly strong WPSH variations during the developing phase of the CP-II El Niño.

We next use the four mechanism indices described in Data and Methods to examine the impact mechanisms in the hindcasts during the three types of El Niño. Figure 3 compares the hindcasted and observed mechanism indices for the three types of El Niño. For the EP El Niño (Fig. 3a-d), the NWP-II mechanism (which involves the two-step Gill response) is the key contributor to the observed El Niño impacts on the WPSH during peak winter, while the IOC mechanism is the key contributor to the decaying summer

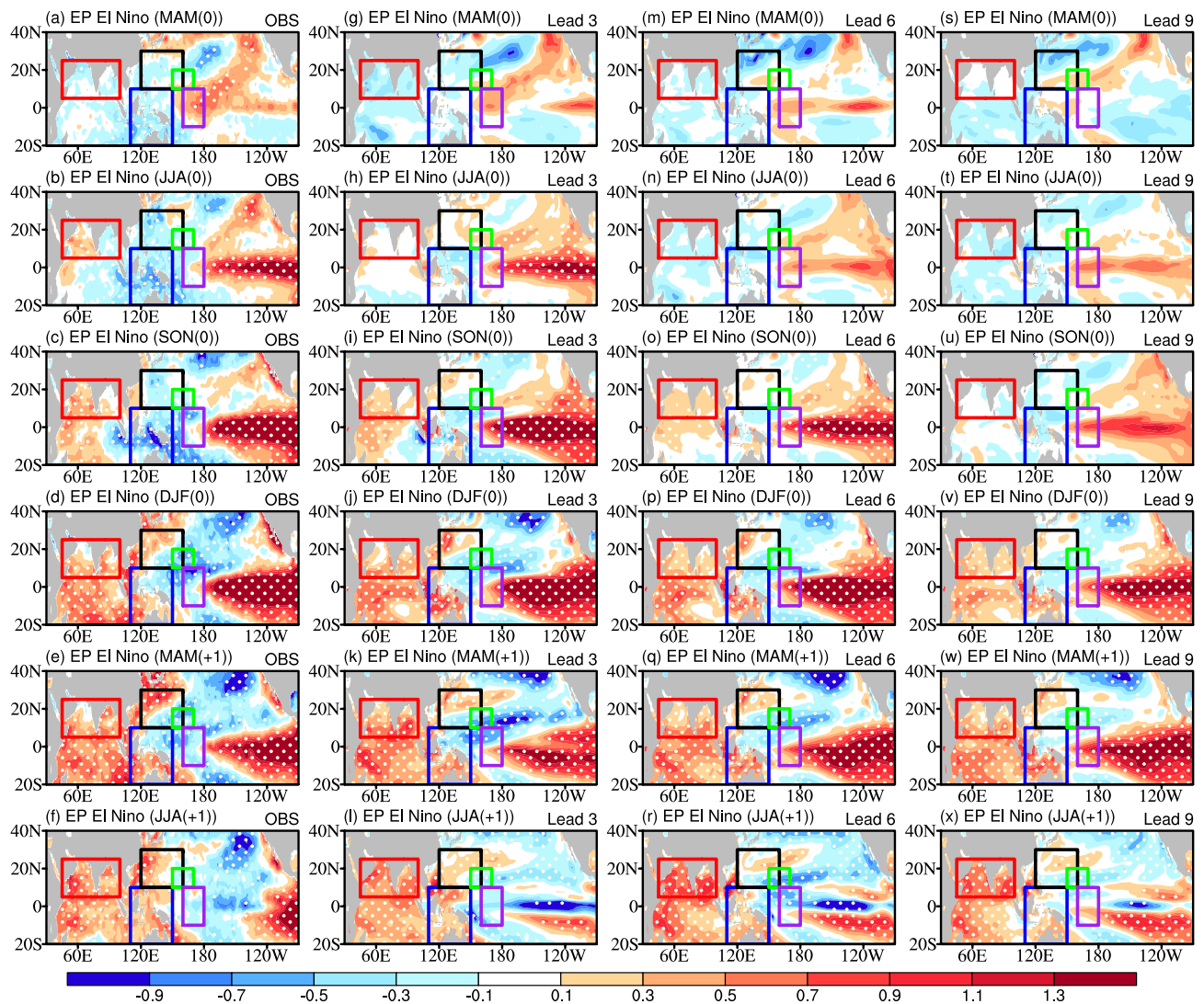


Fig. 4 Evolution of composite EP El Niño SST anomalies (shaded, unit: $^{\circ}\text{C}$) in the observations (1st column) and the hindcasts at 3-month lead (2nd column), 6-month lead (3rd column), and 9-month lead (4th column). The evolution spans from El Niño's developing summer (JJA (0)), developing autumn (SON (0)), peak winter (DJF (0)), decaying spring (MAM (1)), to decaying summer (JJA (1)). The

color boxes mark the regions where the following indices are defined: black (WPSH index), purple (NWP-I index), green (NWP-II index), blue (MC index), and red (IOC index). Dots represent regions where the composite anomalies exceed the 90% significance level using a Student's t test

impacts. The hindcasts overall produce reasonably realistic IOC and NWP-II mechanisms except during the decaying spring and summer when the NWP-II mechanism is overestimated. This overestimation is partially cancelled out by the NWP-I mechanism. Therefore, the NWP coupling mechanism (i.e., NWP-I plus NWP-II) is not the primary cause for the overestimation of the EP El Niño impact on the WPSH during decaying summer we identified in Fig. 2. The primary cause is the large overestimation of the MC mechanism. The hindcasted MC index is two to three times larger than that observed throughout most of the lifecycle of the EP El Niño. We conclude from the comparisons that an overestimated MC mechanism, together with the overestimation of the IOC and NWP-II mechanisms, leads to the overestimated impact on the WPSH during the decaying summer of EP El Niños.

For the CP-I El Niño (Fig. 3e–h), the hindcasted mechanism indices in general align with the observed ones. This explains why the hindcasted WPSH variations during the CP-I El Niño are similar to the observed variations (see Fig. 2e). In both the observations and the hindcasts, the two strongest impact mechanisms are the positive IOC mechanism and the negative NWP-I mechanism. These two terms basically cancel out each other and this partially explains why the CP-I El Niño produces weak impacts on the WPSH as noted in Fig. 2e. For the CP-II El Niño (Fig. 3i–l), in the observations, the NWP-II and MC mechanisms are the key contributors to the WPSH impacts during the peak winter and decaying summer. The hindcasts' overestimation of the WPSH impacts during the developing autumn and early winter is primarily related to an overestimation of the IOC mechanism during those seasons.

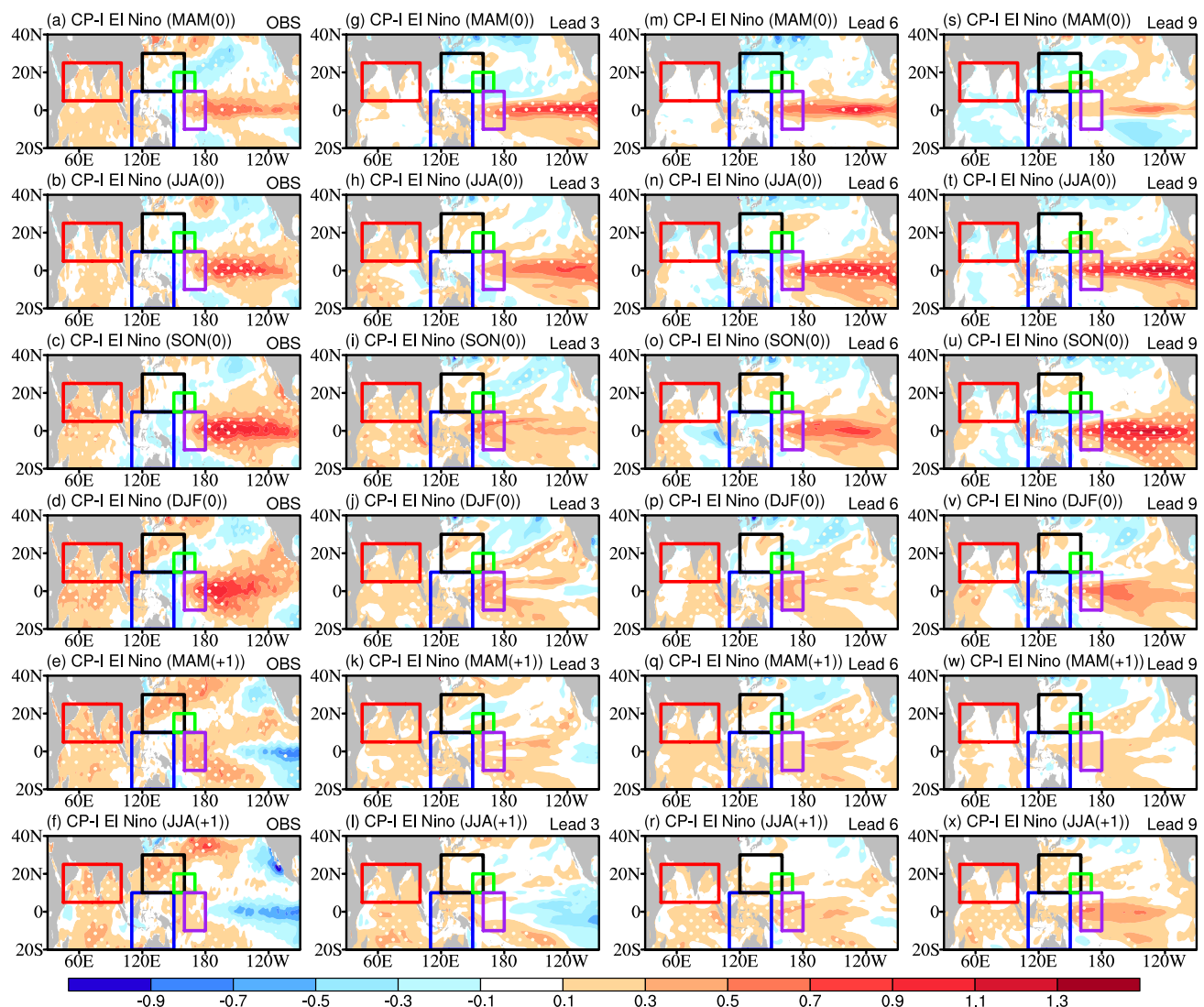


Fig. 5 Same as Fig. 4 but for the CP-I El Niño

The analyses shown in Fig. 3 indicate that the biggest cause for the hindcast errors in WPSH impacts is the MC mechanism for the EP El Niño during decaying summer and the IOC mechanism for the CP-II El Niño during the developing autumn and winter. As discussed in Chen et al. (2019), these two mechanisms are associated with the El Niño-induced SST anomaly pattern in the Indian Ocean and around the MC region. Therefore, we compare in Figs. 4, 5, 6 the composite SST anomalies for the EP, CP-I and CP-II El Niño in the hindcasts and the observations. During the EP El Niño, anomalous warming is observed to develop from the South American coast toward the central Pacific during the developing seasons and peak winter and then retreat back to the coast during the decaying summer (Fig. 4a–f). In the MC region, anomalous cooling during the developing and peak phases is replaced by warming during the decaying summer. Associated with this sign change in the SST anomalies, the

MC mechanism index switches from negative values to positive values during the decaying summer (see Fig. 3b). In the Indian Ocean, El Niño-induced warming is observed from the developing summer to decaying summer. This explains the positive values of the IOC mechanism index throughout most of the EP El Niño (see Fig. 3a).

The hindcasts basically reproduce the observed Pacific warming during the EP El Niño at all lead times (Fig. 4g–x). The model performance is further examined in Fig. 7 with the pattern correlations between the observed and hindcasted SST anomalies. The pattern correlations were calculated separately for the SST anomalies in the tropical Pacific and tropical north Indian Ocean from the developing to decaying years of the three types of El Niño. The correlations indicate that the hindcasted SST anomalies in the tropical Pacific resemble highly with the observations during the developing and peak phases of the EP El Niño. The correlation

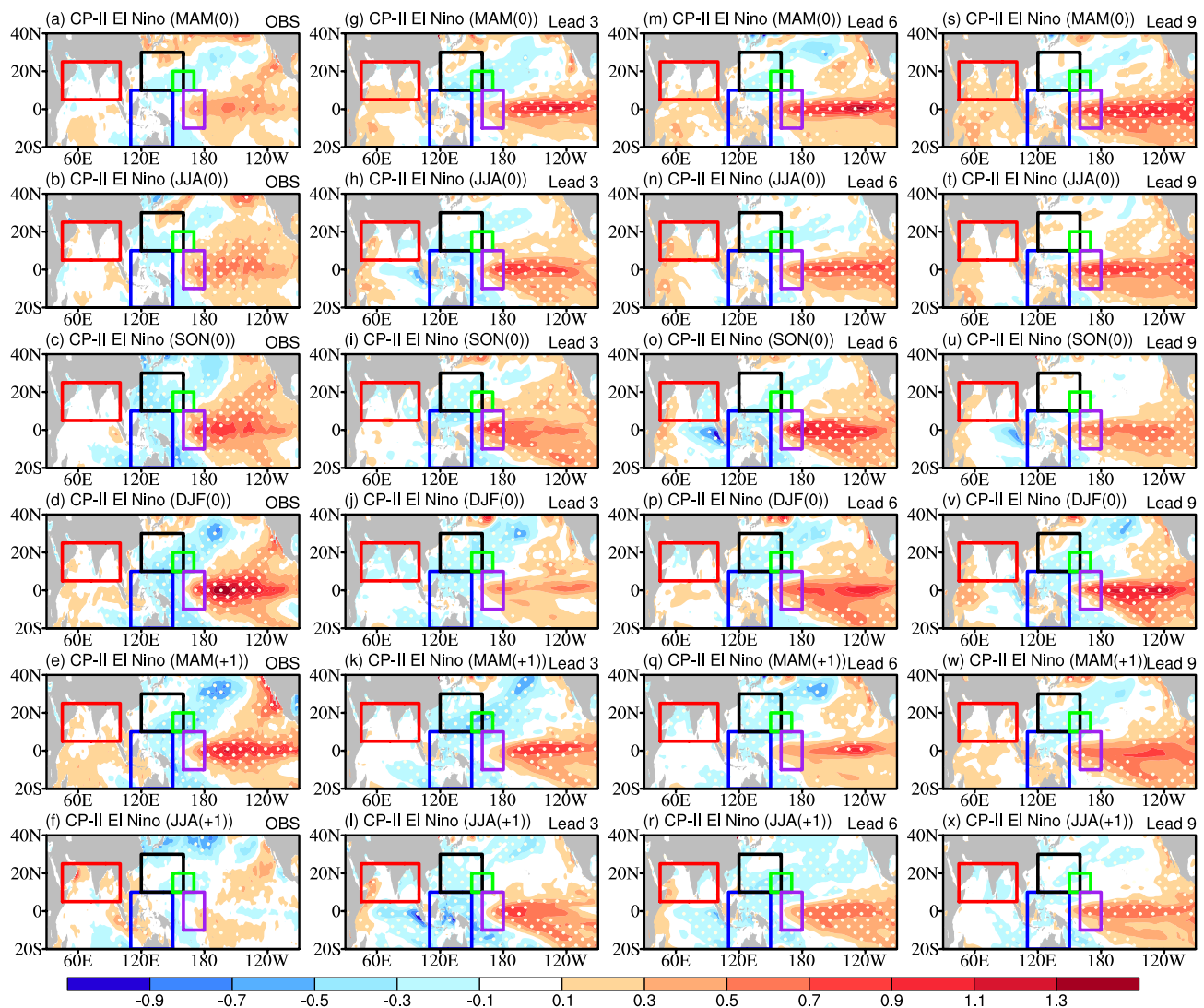


Fig. 6 Same as Fig. 4 but for the CP-II El Niño

coefficients range in 0.6–0.9 during these two phases at all leads (Fig. 7a). However, the pattern correlations decrease during the decaying phase (i.e., MAM and JJA) for the longer-lead hindcasts. From Fig. 4, we notice that the warm center of the hindcasted EP El Niño extends more westward than the observed. The westward extension leads to an erroneous warming in the tropical central Pacific near the NWP-I index region. This erroneous warming can be more obviously seen in Fig. 8, which displays the SST and 850 hPa wind anomaly differences between the hindcasted and the observed EP El Niño. This figure shows that an erroneous

warming begins to appear in the NWP-I index region during the developing autumn and peak winter and lasts to the decaying spring and summer. The error is particularly large in the lead-9 month hindcast (Fig. 8u–x) and explains why the Pacific pattern correlation in Fig. 7 drops significantly for this hindcast during the decaying phase of the EP El Niño. Previous studies have shown that an anomalous warming in the tropical central Pacific can excite an anomalous cyclonic circulation in the NW Pacific via a Gill response (Fan et al. 2013). Such an anomalous cyclone induced by the erroneous warming is evident in the 850 hPa wind anomaly differences

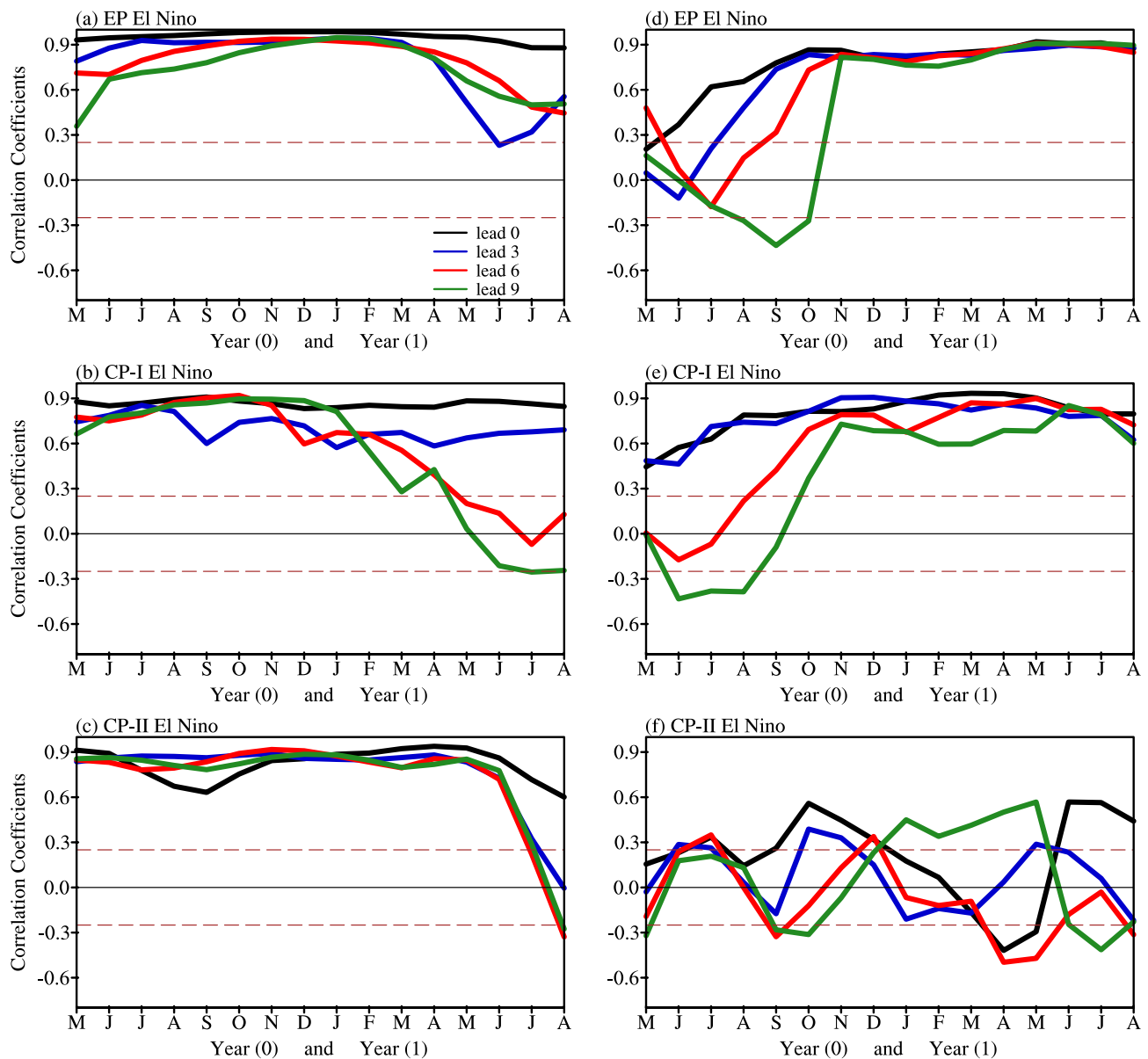


Fig. 7 Pattern correlation coefficients between the hindcasted and observed SST anomalies in the tropical Pacific (25° S– 25° N, 150° E– 90° W) (left panel) and North Indian Ocean (5° – 25° N, 40° – 100° E) (right panel) from the developing to decaying years of three types of

El Niño. In each panel, black lines are for the lead-0 month hindcasts, blue lines for the lead-3 month hindcasts, red lines for lead-6 month hindcasts, and green lines for the lead-9 month hindcasts. The brown-dotted lines indicate the 90% confidence level

of Fig. 8u–x. This anomalous cyclone can directly weaken the WPSH. This explains why the NWP-I mechanism index in the hindcasts is weaker than that observed (see Fig. 3c). The anomalous cyclone can also decrease the anomalous warming underneath via local air-sea interactions. This weaker anomalous warming can be revealed by comparing, for example, the 9-month hindcasted and observed SST anomalies in the WPSH region during the decaying spring and summer (cf. Fig. 4e–f and w–x and their differences in Fig. 8w–x). This weaker warming subsequently causes the MC mechanism index to be overestimated in the hindcasts (see Fig. 3b), because this mechanism index is defined as

the vertical velocity difference between the WPSH region and the MC region. In the tropical north Indian Ocean, the hindcasted EP El Niño resemble highly with the observations from the developing autumn to the decaying summer (see Figs. 4 and 8). The pattern correlations between the hindcasted and observed SST anomalies stay around 0.9 during these phases at all lead months (Fig. 7d). The pattern correlations are low only during the developing spring and summer, when the IOC mechanism is not important to the WPSH variations (see Fig. 3a). In conclusion, a too-westward shifted El Niño SST anomalies cause the hindcasts to produce overly strong MC mechanism, which contributes to

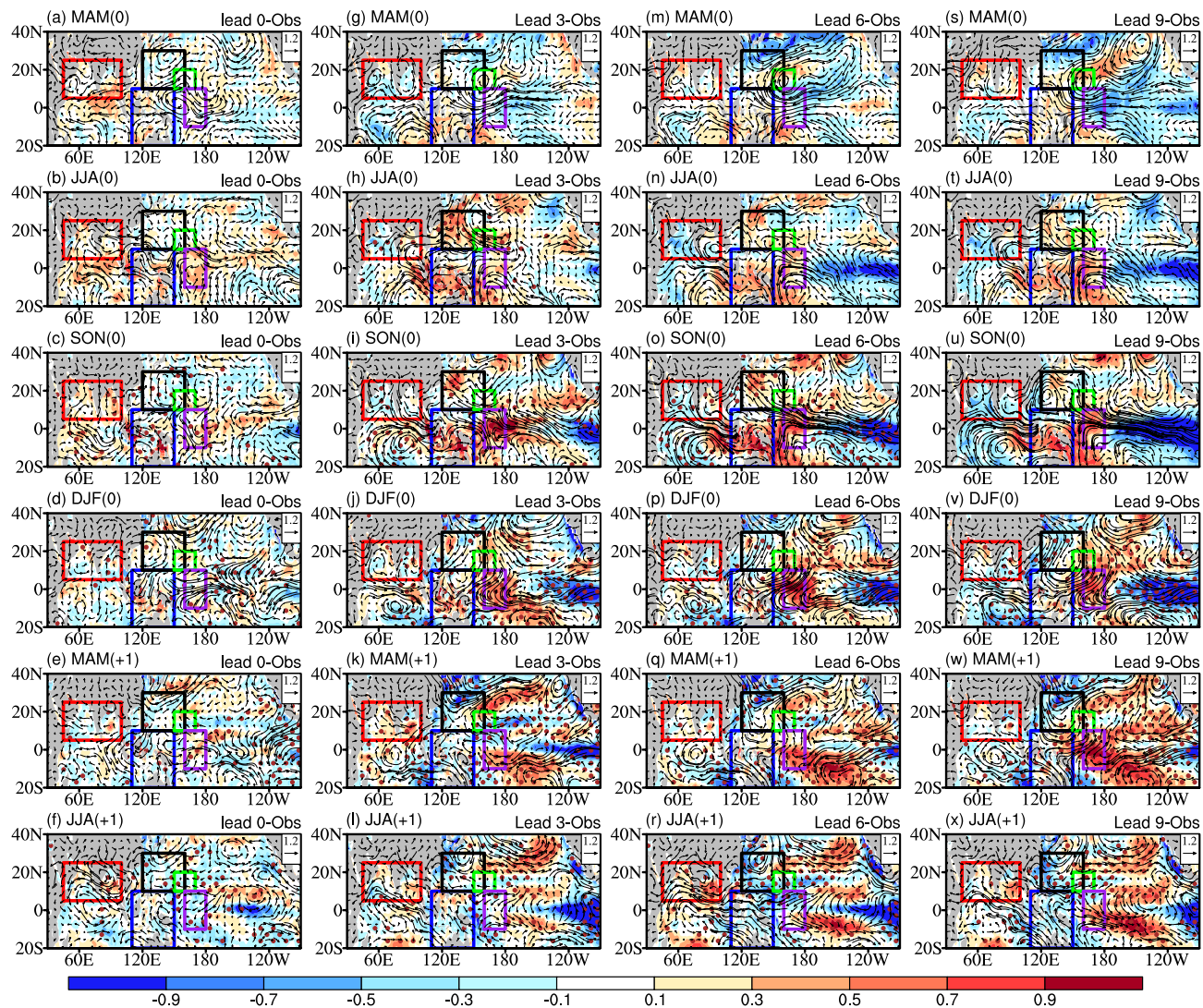


Fig. 8 Differences between composited EP El Niño 850 hPa wind (vector, unit: m/s) and SST anomalies (shaded, unit: °C) in the 0-month lead (1st column), 3-month lead (2nd column), 6-month lead (3rd column), and 9-month lead (4th column) and the observations. The evolution spans from El Niño's developing spring (MAM (0); 1st row), summer (JJA (0); 2nd row), developing autumn (SON (0); 3rd row), peak winter (DJF (0); 4th row), decaying spring (MAM (+1); 5th

row), to decaying summer (JJA (1); 6th row). The color boxes mark the regions where the following indices are defined: black (WPSH index), purple (NWP-I index), green (NWP-II index), blue (MC index), and red (IOC index). Dots represent regions where the differences of composite SST anomalies exceed the 95% significance level using a Student's *t* test

an overestimation of the WPSH variations during the decaying summer of the EP El Niño.

During CP-I El Niños, the observed SST anomalies (Fig. 5a–f) are weaker than those during EP El Niños. Thus, the intensities of the four impact mechanisms are weaker than during EP El Niños (Fig. 3e–h). Significant warming is observed in the tropical central Pacific near the NWP-I region and in the Indian Ocean throughout CP-I El Niños. Warming in the former region weakens the WPSH through the one-step Gill response (associated with a negative NWP-I index; see Fig. 3g), which cancels out the strengthening effect on the WPSH produced by the IOC mechanism (see Fig. 3e). The hindcasts reproduce these two key features of SST anomalies during the CP-I El Niño at all lead times

(Fig. 5g–x), although minor discrepancies exist. The most noticeable discrepancy is that the hindcasts (except at the 3-month lead) did not produce the observed transition into a cold phase after the El Niño decays (Fig. 5e–f). Thus, the negative impacts induced by the negative SST anomalies in the eastern equatorial Pacific via the two-step Gill response (i.e., the NWP-II mechanism) in the hindcasts is slightly weaker than the observed (Fig. 3h). The hindcasted warm bias in the tropical eastern Pacific during the decaying summer can be clearly seen in the SST difference maps of Fig. 9. This warm bias also causes the Pacific pattern correlation to degrade to small values in Fig. 7b. The pattern correlations in the tropical north Indian Ocean (Fig. 7e) indicates that the hindcasted CP-I El Niño has a reasonably realistic SST

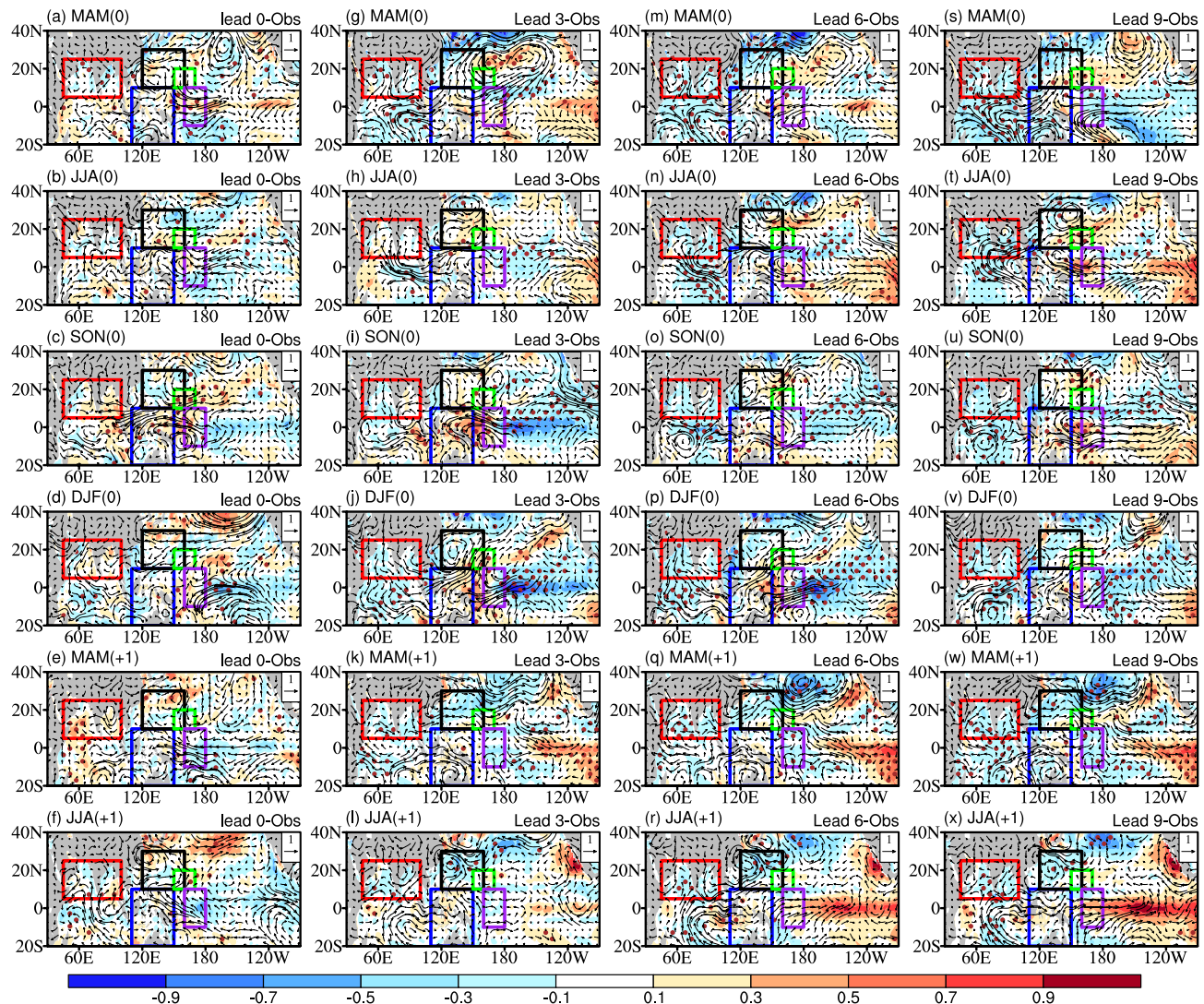


Fig. 9 Same as Fig. 8 but for the CP-I El Niño

anomaly pattern in the Indian Ocean. The pattern correlation is low only during the developing spring and summer. During the developing autumn and peak winter when the strongest WPSH response to the CP-I El Niño occurs, the hindcasts produce realistic SST anomalies in both the tropical Pacific and north Indian Oceans. This explains why the hindcasts realistically simulate the impacts on the WPSH during the CP-I El Niño.

During CP-II El Niños, the observed SST anomaly evolution is similar to that observed during CP-I El Niños with two important exceptions. As mentioned, the first exception is that the tropical central Pacific warming during CP-II El Niños is accompanied by significant anomalous warming over the northeastern subtropical Pacific during the developing phase. CP-I El Niños produces the tropical central Pacific warming but not the subtropical Pacific warming. The second difference is that the CP-I El Niño is

accompanied with a significant Indian Ocean warming, but the Indian Ocean warming is very weak during the CP-II El Niño. The weak Indian Ocean warming observed during the CP-II El Niño explains the very weak IOC mechanism in Fig. 3i. The pattern correlations shown in Fig. 7c and f indicate that the hindcasted CP-II El Niño simulates the Pacific SST anomaly pattern realistically but not the Indian Ocean SST anomaly pattern. The Pacific pattern correlations between the hindcasted and observed CP-II El Niño are close to 0.9 at all leads from the developing spring to the decaying spring. In contrast, the pattern correlations for the Indian Ocean SST anomalies are very low throughout the lifecycle of the CP-II El Niño. Figure 6 shows that the hindcasts reproduce the observed anomalous warming in the tropical central Pacific and northeastern subtropical Pacific at all lead times. However, SST anomalies in the Indian Ocean appear to be stronger in the hindcasts than in

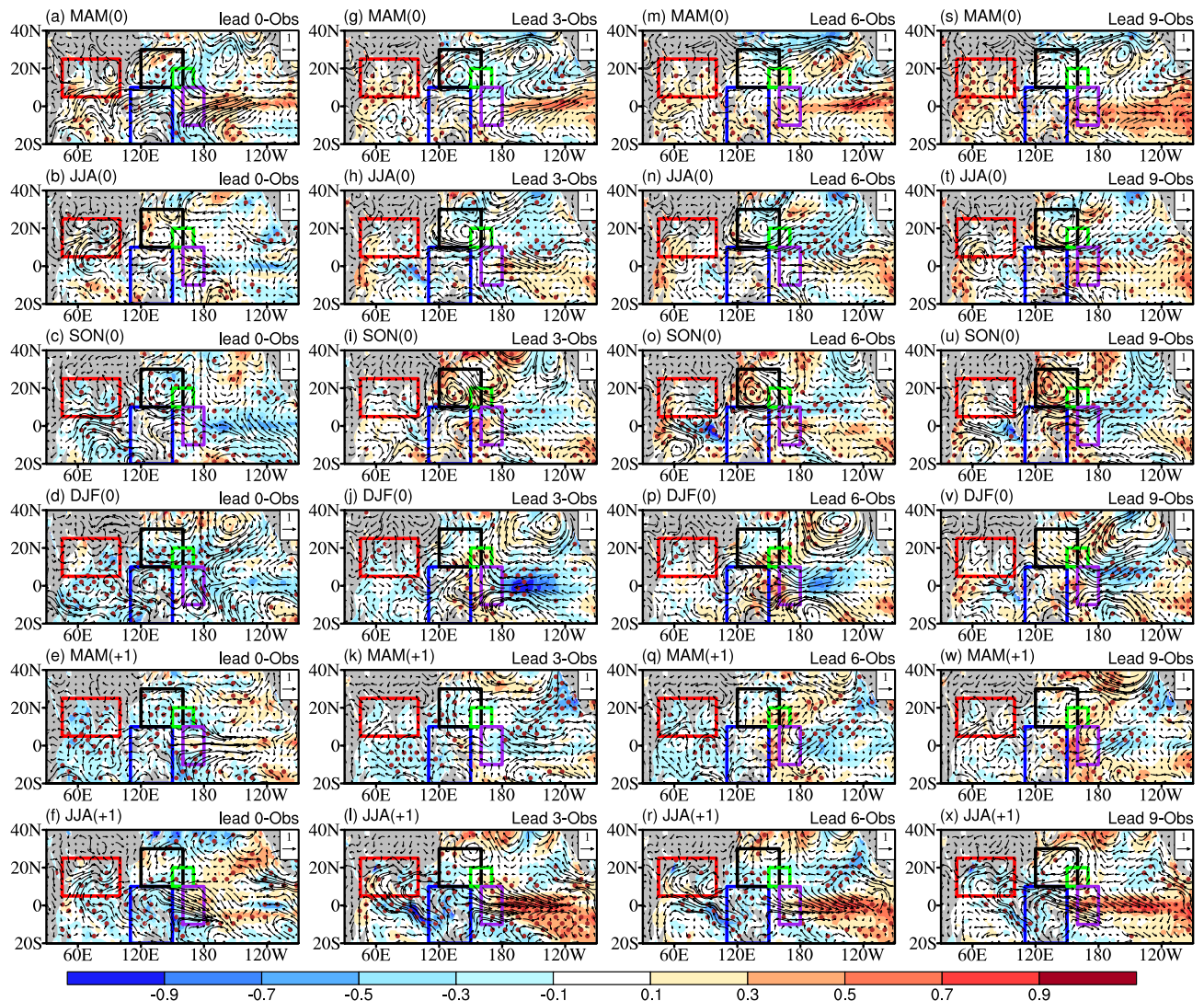


Fig. 10 Same as Fig. 8 but for the CP-II El Niño

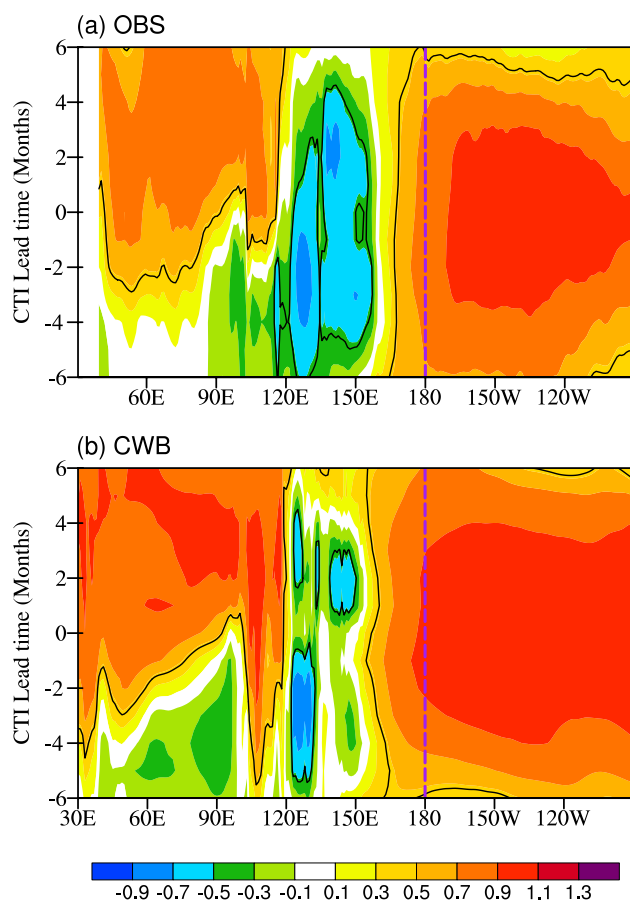


Fig. 11 Lead-lagged correlation coefficients between the Cold Tongue Index (CTI) in November–December–January (NDJ) and the Indo-Pacific SST anomalies along the equatorial (5° N and 5° S) calculated from the (a) observations, (b) ensemble mean of CWB hindcasts from 0-month to 9-month leads. The dashed-purple lines mark the International Dateline

the observations. The SST anomaly differences between the hindcasted and observed CP-II El Niño (Fig. 10) reveal that the differences in the Indian Ocean are particularly large from the developing spring to the developing autumn. The erroneous Indian Ocean warming can excite atmospheric Kelvin waves (see the anomalous easterlies in the western Pacific of Fig. 10s–u) propagating eastward to strengthen the WPSH. These seasons are close to the time when the IOC mechanism is overestimated in Fig. 3i. Therefore, a slightly

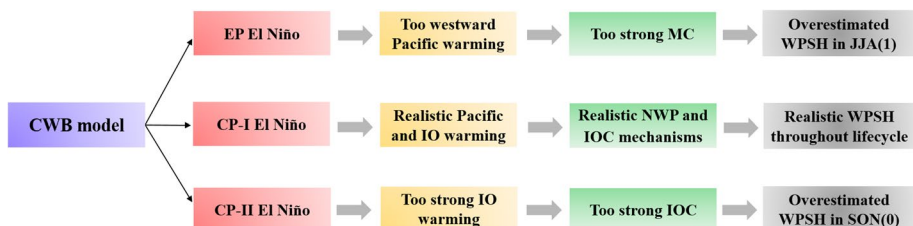
(but statistically significant) stronger response in the Indian Ocean is the reason why the CWB model hindcasts overestimate the impact of the CP-II El Niño on the WPSH during the developing autumn and peak winter.

4 Sources of model biases

The above analyses suggest that the westward shift in the El Niño SST anomalies and the overly strong Indian Ocean warming induced by the El Niño are key biases of the CWB model that affect its hindcasts of the impacts of the three types of El Niño on the WPSH. To further confirm these two model biases, we show in Fig. 11 the observed and hindcasted structures and evolutions of the equatorial SST anomalies. The values shown are the lead-lagged correlation coefficients between the CTI index in November–December–January (NDJ) and the Indo-Pacific SST anomalies along the equatorial (between 5° N and 5° S). In both the observations (Fig. 11a) and hindcasts (Fig. 11b), the coefficients reveal the typical SST anomalies associated with El Niño that are characterized by anomalous warming in the tropical eastern and central Pacific, anomalous cooling in the tropical western Pacific around the MC region, and lagged anomalous warming in the Indian Ocean. However, it is evident that the Pacific warming extends further westward in the hindcasts (to 150° E) (Fig. 11b) than in the observations (160° E) (Fig. 11a), and that the lagged Indian Ocean warming is stronger in the hindcasts than in the observations.

The westward extension in El Niño SST anomalies is a common model deficiency shared by a number of contemporary coupled atmosphere–ocean models (Yang and Giese 2013; He et al. 2020; Wang et al. 2019). In a recent study, He et al. (2020) showed that the westward extension of SST anomalies causes the model Walker circulation to shift further into the Indian Ocean than in the observations. As a result, the model El Niño induced warming in the Indian Ocean is stronger than the observed. Their finding suggested that the too-westward extension of SST anomalies and the overly strong Indian Ocean warming are two related model deficiencies. According to He et al. (2020), the westward-expanded Walker circulation affects surface heat fluxes to induce stronger Indian Ocean warming. The present study suggests that this overly strong warming results in an overly strong IOC

Fig. 12 Schematics illustrate the causes of CWB model errors in hindcasting the three types of El Niño on WPSH



mechanism to cause climate models to overestimate the El Niño impacts on the WPSH.

5 Conclusions and discussions

Observational studies have shown that the three types of El Niño (the EP El Niño, CP-I El Niño and CP-II El Niño) produce dramatically different impacts on the WPSH (Chen et al. 2019). This study assesses the ability of the CWB hindcast model in reproducing the impacts of the different El Niños on the WPSH. Although the study was conducted with one specific model, the results identify model deficiencies that are known to be common among contemporary climate models. The evaluation in this study indicates that the CWB model predicts an overly strong delayed impact of the EP El Niño on WPSH and an overly strong developing impact of the CP-II El Niño on the WPSH. The model is able to reasonably simulate the CP-I El Niño impacts on the WPSH. This finding indicates that it is necessary and useful for forecasters to identify the El Niño type to make better use of the predictions. Since the El Niño type can be determined very early in the development of an event based on the location of the SST anomalies, forecasters can use this information to determine the reliability of the model forecasts of the WPSH variations. For example, based on our results, the CWB model forecasts of future WPSH variations are likely to be accurate throughout the lifecycle of a CP-I El Niño event, during the developing and peak seasons of an EP El Niño event, and during the peak and decaying seasons of a CP-II El Niño event. The forecasted WPSH variations tend to be overestimated (and thus need to be adjusted downward) during the decaying summer of an EP El Niño and during the developing autumn and early winter of a CP-II El Niño event.

This study also identifies key impact mechanisms that cause the model errors in predicting the diverse El Niño impacts on the WPSH (summarized in Fig. 12). For the EP El Niño, an overly strong MC circulation mechanism causes an overestimation of WPSH variations during the decaying summer. The error in this mechanism was further attributed to an erroneous westward extension of the mode El Niño SST anomalies. For the CP-II El Niño, the overly strong IOC mechanism is responsible for model errors in predicting the El Niño impact on WPSH variations during the developing autumn. The overly strong IOC mechanism is attributed to overly strong Indian Ocean warming. The model produces reasonable predictions of the impacts of the CP-I on the WPSH. This study further finds that the erroneous westward extension of SST anomalies in the Pacific and the overly strong Indian Ocean warming to be related. Thus, the model deficiency in simulating the correct El Niño SST

anomaly location needs to be alleviated to improve model performance in simulating WPSH variations, which play an important role in modulating weather and climate in the Western Pacific and East Asian regions.

Acknowledgements We thank two anonymous reviewers for their valuable comments. This research was supported by the Central Weather Bureau of Taiwan through a contract to University of California, Irvine. Jin-Yi Yu is also supported by NSF's Climate & Large-scale Dynamics Program under Grants AGS-1833075. The SST data of the Hadley Center Sea Ice and Sea Surface Temperature dataset were downloaded from their website (<https://www.metoffice.gov.uk/hadobs/hadisst/data/download.html>). The monthly SLPs, winds and Omega fields of National Centers for Environmental Prediction/National Center for Atmospheric Research (NCEP/NCAR) were obtained from NOAA (<https://www.esrl.noaa.gov/psd/>).

References

- Chang CP, Zhang Y, Li T (2000) Interannual and interdecadal variations of the East Asian summer monsoon and tropical Pacific SSTs. Part I: Roles of the subtropical ridge. *J Clim* 13:4310–4325
- Chen M, Yu JY, Wang X, Jiang W (2019) The changing impact mechanisms of a diverse El Niño on the western Pacific subtropical high. *Geophys Res Lett* 46:953–962
- Du Y, Yang L, Xie SP (2011) Tropical Indian Ocean influence on Northwest Pacific tropical cyclones in summer following strong El Niño. *J Clim* 24:315–322
- He S, Yu JY, Yang S, Fang SW (2020) ENSO's impacts on the tropical Indian and Atlantic Oceans via tropical Processes: CMIP5 simulations versus observations. *Clim Dyn.* <https://doi.org/10.1007/s00382-020-05247-w>
- Ho CH, Baik JJ, Kim JH, Gong DY et al (2004) Interdecadal changes in summertime typhoon tracks. *J Clim* 17:1767–1776
- Jiang W, Huang G, Hu K, Wu R et al (2017) Diverse relationship between ENSO and the northwest Pacific summer climate among CMIP5 models: dependence on the ENSO decay pace. *J Clim* 30:109–127
- Jiang W, Huang G, Huang P, Hu K (2018) Weakening of Northwest Pacific Anticyclone Anomalies during Post-El Niño Summers under Global Warming. *J Clim* 31:3539–3555
- Kalnay E, Kanamitsu M, Kistler R et al (1996) The NCEP/NCAR 40-year reanalysis project. *Bull Am Meteorol Soc* 77:437–471
- Kao HY, Yu JY (2009) Contrasting eastern-pacific and central-pacific types of ENSO. *J Clim* 22:615–632
- Kumar A, Hoerling MP (2003) The nature and causes for the delayed atmospheric response to El Niño. *J Clim* 16:1391–1403
- Lau KM, Kim KM, Yang S (2000) Dynamical and boundary forcing characteristics of regional components of the Asian summer monsoon. *J Clim* 13:2461–2482
- Lee EJ, Jhun JG, Park CK (2005) Remote connection of the northeast Asian summer rainfall variation revealed by a newly defined monsoon index. *J Clim* 18:4381–4393
- Matsumura S, Sugimoto S, Sato T (2015) Recent intensification of the western pacific subtropical high associated with the east asian summer monsoon. *J Clim* 28:2873–2883
- Paek H, Yu JY, Hwu JW, Lu MM et al (2015) A source of AGCM bias in simulating the western Pacific subtropical high: different sensitivities to the two types of ENSO. *Mon Weather Rev* 143:2348–2362

- Paek H, Yu JY, Zheng F, Lu MM (2019) Impacts of ENSO diversity on the western Pacific and North Pacific subtropical highs during boreal summer. *Clim Dyn* 52:7153–7172
- Park JY, Jhun JG, Yim SY, Kim WM (2010) Decadal changes in two types of the western North Pacific subtropical high in boreal summer associated with Asian summer monsoon/El Niño-Southern Oscillation connections. *J Geophys Res* 115:D21129
- Rayner NA, Parker DE, Horton EB et al (2003) Global analyses of sea surface temperature, sea ice, and night marine air temperature since the late nineteenth century. *J Geophys Res* 108(D14):4407
- Stowasser M, Wang Y, Hamilton K (2007) Tropical cyclone changes in the western North Pacific in a global warming scenario. *J Clim* 20:2378–2396
- Sui CH, Chung PH, Li T (2007) Interannual and interdecadal variability of the summertime western North Pacific subtropical high. *Geophys Res Lett* 34:L11701
- Tan W, Wang X, Wang W, Wang C et al (2016) Different responses of sea surface temperature in the South China Sea to various El Niño events during boreal Autumn. *J Clim* 29:1127–1142
- Wang B, Wu R, Fu X (2000) Pacific-East Asian teleconnection: how does ENSO affect East Asian climate? *J Clim* 13:1517–1536
- Wang B, Zhang Q (2002) Pacific-East Asian teleconnection. Part II: how the Philippine Sea anomalous anticyclone is established during El Niño development. *J Clim* 15:3252–3265
- Wu L, Wang B, Geng S (2005) Growing typhoon influence on east Asia. *Geophys Res Lett* 32:L18703. <https://doi.org/10.1029/2005GL022937>
- Wu TY, Juang HMH, Chen YL, Liu PY, Lin SI, Chen JH, Lu, MM (2019) CWB CFS 1-Tier Hindcast Analysis and Forecast Verification. Climate Prediction S&T Digest, p.172.
- Wang CZ, Wang X (2013) Classifying El Niño Modoki I and II by different impacts on rainfall in southern China and typhoon tracks. *J Clim* 26:1322–1338
- Wang X, Chen M, Wang C, Yeh SW et al (2019) Evaluation of the relationships between the North Pacific oscillation and El Niño Modoki in CMIP5 models. *Clim Dyn* 52:1383–1394
- Xie SP, Hu K, Hafner J, Tokinaga H et al (2009) Indian Ocean capacitor effect on Indo-western Pacific climate during the summer following El Niño. *J Clim* 22:730–747. <https://doi.org/10.1175/2008JCLI2544.1>
- Xie SP, Kosaka Y, Du Y, Hu KM et al (2016) Indo-western Pacific ocean capacitor and coherent climate anomalies in post-ENSO summer: a review. *Adv Atmos Sci* 33(4):411–432. <https://doi.org/10.1007/s00376-015-5192-6>
- Yang C, Giese BS (2013) El Niño Southern Oscillation in an ensemble ocean reanalysis and coupled climate models. *J Geophys Res* 118:4052–4071
- Yu JY, Kao HY (2007) Decadal changes of ENSO persistence barrier in SST and ocean heat content indices: 1958–2001. *J Geophys Res* 112:D13106

Publisher's Note Springer Nature remains neutral with regard to jurisdictional claims in published maps and institutional affiliations.